Chalcogenide Letters Vol. 22, No. 10, October 2025, p. 917 - 927

Theoretical exploration of the structure and physical properties of $AgAlSe_2$

T. J. Li [a,*], Y. Yue [a], L. P. Qu [a], H. J. Hou [b], S. H. Fan [b], H. L. Guo [c], S. R. Zhang [d]
[a] *Institute of Automotive and Traffic Engineering, Yancheng Polytechnic College, Yancheng 224005, China*
[b] *School of Materials Engineering, Yancheng Institute of Technology, Yancheng, 224051, China*
[c] *College of Electronic and Information Engineering, Yangtze Normal University, Fuling, 408000, Chongqing, China*
[d] *School of Physics, Electronics and Intelligent Manufacturing, Huaihua University, Huaihua, 418008, China*

The material $AgAlSe_2$, which adopts a chalcopyrite crystal structure, has attracted significant attention owing to its promising functional properties. To further explore its characteristics, theoretical method was conducted to explore its elastic behavior, electronic structure, dynamic stability, and thermodynamic features. The lattice parameters and elastic constants obtained through simulation agrees well with the reported data. Additionally, the mechanical stability of $AgAlSe_2$ was assessed through its elastic constants, confirming its structural integrity. Electronic property analysis reveals that $AgAlSe_2$ exhibits semiconducting behavior, featuring a direct band gap of approximately 1.1377 eV.

(Received July 4, 2025; Accepted October 29, 2025)

Keywords: $AgAlSe_2$, Electronic properties, Mechanical, Dynamical, Thermodynamics

1. Introduction

In recent years, increasing interest has been directed towards materials like ternary chalcopyrite compounds. Notable examples include $AgXY_2$, where X can be Al, Ga, or In and Y refers to S, Se, or Te. Another category is ABX_2, where A may be Cu or Ag, B can be In, Ga, or Al, and X stands for Se or S. These materials are regarded as promising candidates for optical applications [1-8]. Among these compounds, $AgAlSe_2$ emerges as a semiconductor with a chalcopyrite-like structure. It exhibits a distinct point group symmetry and falls under the space group I-42d [9]. At present, $AgAlSe_2$ has garnered considerable scientific attention, prompting numerous studies into its characteristics. Maeda et al. conducted an extensive investigation into the physical properties of $CuInSe_2$ and other related ABX_2 materials, where A = Cu or Ag, B = In, Ga, or Al, and X= Se or S [10]. Utilizing the rigid ion model, A.K. Kushwaha systematically calculated the phonon frequencies and elastic behaviors of chalcopyrite-type materials [11]. S. Mishra analyzed the structural and electronic features of $AgAlX_2$ (X = S, Se, Te) therotical method [12].

* Corresponding author: litj1021@126.com
https://doi.org/10.15251/CL.2025.2210.917

Ullah et al. explored the physical properties of Ag-based ternary compounds [13]. Sharan et al. studied the electronic configuration and other properties of oxygen vacancy compounds, along with their associated physical properties, through theoretical approaches [14]. In this study, we compute and evaluate the band structure, elastic behavior, dynamic characteristics, and thermodynamic properties of $AgAlSe_2$ primarily by employing first-principles calculations. Although $AgAlSe_2$ holds potential for technological applications, only its structural features have been experimentally explored to date. Here, we focus on examining its elastic and electronic properties to better understand its applicability.

2. Calculation methods

All computations were carried out using the Projected Augmented Wave (PAW) method[15], implemented within the VASP software suite [16]. The exchange-correlation functional was treated under the Generalized Gradient Approximation, specifically in the Perdew-Burke-Ernzerhof (PBE) formulation [17]. To investigate the band structure and dynamic behavior of $AgAlSe_2$, a *k*-point mesh of 5×5×5 and a energy cutoff of 500 eV was utilized. The vibrational properties were determined through calculations performed with the Phonopy package [18]. For enhanced accuracy in the phonon computations, a 2×2×1 supercell comprising 64 atoms in total was created before conducting the dynamic analysis.

3. Results and discussion

3.1. Structural properties of $AgAlSe_2$

$AgAlSe_2$ exhibits a specific point group symmetry and is assigned to the space group I-42d and adopts a chalcopyrite-type crystal structure. The atomic arrangement of $AgAlSe_2$ is plotted in Fig. 1. The lattice constants of $AgAlSe_2$ is presented in Table 1. By comparison, it is found that they are highly consistent with the previous experimental measurement results [19] as well as the previous reported theoretical results [12, 13]. While minor discrepancies are present in some parameter values, the differences remain within 2%. These small deviations may be attributed to the use of the GGA approximation during structural relaxation.

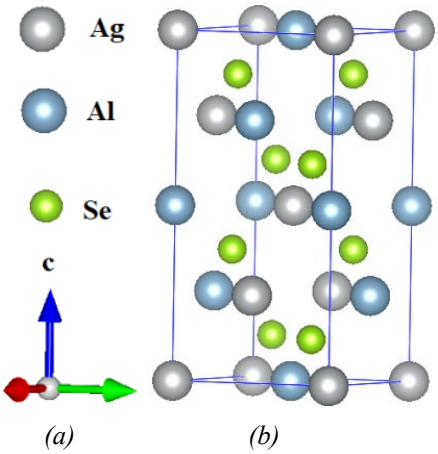

Fig. 1. Crystal model of $AgAlSe_2$.

Table 1. The equilibrium structural parameters (a, c) (Å), c/a of $AgAlSe_2$.

	a (Å)	*c* (Å)	*c*/*a*
Present	6.0416	11.1233	1.8411
Theor.[12]	5.78	11.92	2.0622
Theor.[13]	5.935	10.991	1.8519
Exp.[19]	5.956	10.75	1.8049

3.2. Electronic properties

As demonstrated in Figs. 2 and 3, $AgInSe_2$ behaves as a direct band gap semiconductor, with a bandgap of 1.1377 eV. The band gap of $AgAlSe_2$ was obtained through first-principles computations, with the results presented in Table 2. Although the calculated value is lower than the experimentally reported band gap of 2.55 eV [20], it shows good agreement with previously published theoretical findings [12, 13].

Table 2. Band gap E_g (eV) of $AgAlSe_2$.

	This work	Theo.[12]	Theo. [13]	Theo.[13]	Exp.[20]
$AgInSe_2$	1.1377	1.59	0.8	1.6	2.55

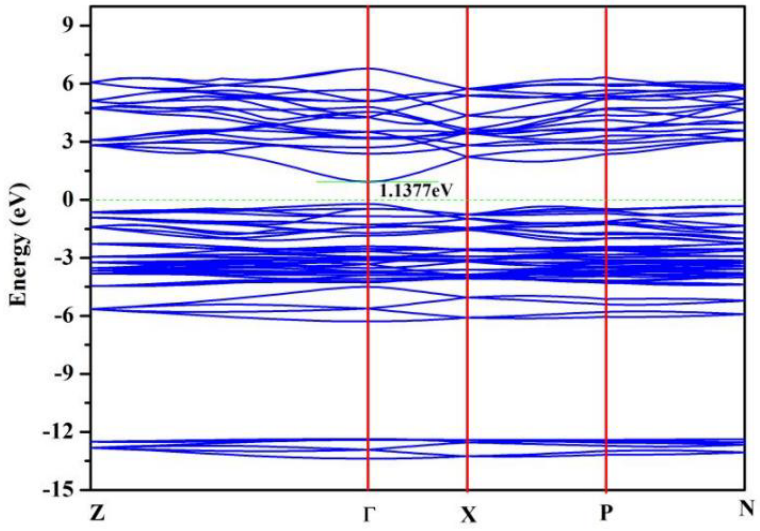

Fig. 2. Band structure of $AgAlSe_2$.

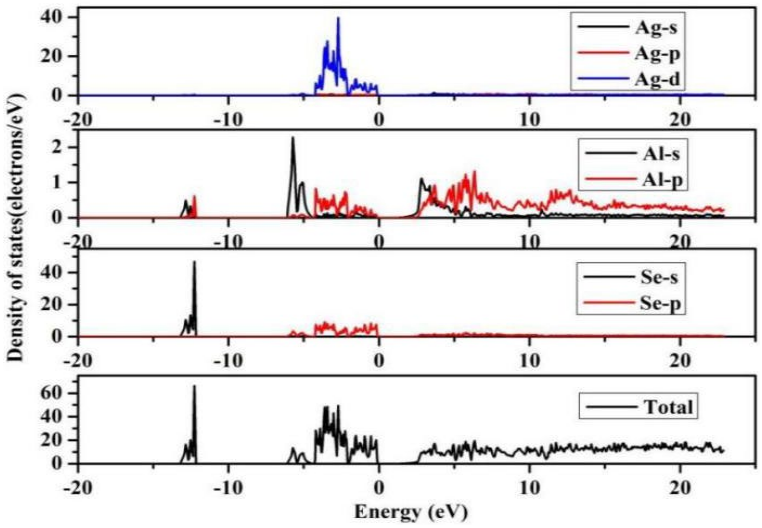

Fig. 3. Density of states of $AgAlSe_2$.

To gain deeper insights into the electronic structure and orbital contributions in $AgAlSe_2$. As shown in Fig. 3 (density of states), the valence band of $AgInSe_2$ is clearly separated into two different regions: photon energies (-15 eV and -10 eV) and (-10 and 0 eV). In energies between -15 eV and -10 eV, strong electron localization arises from the hybridization of Al-s and Se-s orbitals.Within the energy range of -10 to 0 eV, notable electron localization occurs as a result of the hybridization among Ag-d, Al-s, Al-p, and Se-p orbitals. As demonstrated in Figs. 2 and 3, $AgInSe_2$ behaves as a direct band gap semiconductor.

3.3. Elastic properties

$AgAlSe_2$ crystallizes in the chalcopyrite structure. The material's elastic behavior is described by six independent elastic constants, which are conventionally labeled using Young's notation as C_{11}, C_{33}, C_{44}, C_{66}, C_{12}, and C_{13}. Base on the Born stability conditions [21], these elastic constants must satisfy specific criteria.

Table 3. The calculated elastic constants C_{ij} (GPa) of $AgAlSe_2$.

	This work	Theor.[11]	Theor.[22]
C_{11}	70.43	95.6	84.9
C_{33}	63.25	102.4	98.0
C_{44}	22.95	36.1	35.9
C_{66}	25.62	31.5	32.7
C_{12}	44.17	55.7	53.1
C_{13}	44.60	76.3	62.1

As presented in Table 3, the findings of this study closely align with the theoretical values[11, 22]. Furthermore, the fact that the C_{ij} satisfy Born conditions, confirms the structural stability of the compound.

Using these elastic constants C_{ij}, we are able to obtain the elastic anisotropy factor:

$$\alpha_1 = 2C_{44}/(C_{11} - C_{12}) \tag{1}$$

$$\alpha_2 = C_{66}/C_{44} \tag{2}$$

Table 4 clearly shows a considerable difference between the values of a_1 and a_2, indicating that $AgAlSe_2$ possesses pronounced elastic anisotropy.

Furthermore, using the elastic constants C_{ij}, we can also calculatethe linear compressibility in the direction of the *a*-axis and *c*-axis, as well as the overall volumetric compressibility, based on the following expressions. These computed values are also summarized in Table 4 [23].

$$\chi_a = -\frac{1}{a}\frac{\partial a}{\partial p}\bigg|_{p=0} = \frac{C_{33} - C_{13}}{C_{33}(C_{11} + C_{12}) - 2C_{13}^2} \tag{3}$$

$$\chi_c = -\frac{1}{c}\frac{\partial c}{\partial p}\bigg|_{p=0} = S_{33} + 2S_{13} = \frac{C_{11} + C_{12} - 2C_{13}}{C_{33}(C_{11} + C_{12}) - 2C_{13}^2} \tag{4}$$

$$\chi = -\frac{1}{V}\frac{\partial V}{\partial p}\bigg|_{p=0} = 2\chi_a + \chi_c \tag{5}$$

In Table 4, it can be concluded that when pressure is applied to the *a*-axis and *c*-axis of $AgAlSe_2$, the compression effects are comparable.

Table 4. Calculated α_1, α_2, χ_a, χ_c, χ (GPa^{-1}), B (GPa), G (GPa), E (GPa), σ of $AgAlSe_2$.

	α_1	α_2	χ_a	χ_c	χ	*B*	*G*	*E*	*σ*
This work	1.7479	1.1163	0.0057	0.0078	0.0192	52.24	17.89	48.17	0.3463
Theor.[11]						140.25	30.74	85.94	0.3979

In addition, the bulk modulus *B*, shear modulus *G*, Poisson's ratio *σ* and Young's modulus *E* can be obtained from the Voigt and Reuss approximation [24-26]. In Table 4, the values of *B*, *G*, *E*, and *σ* are in good agreement with theoretical data [11]. The *B*/*G* ratio can serve as an indicator to identify whether a material demonstrates brittle/ductile characteristics [27]. In the case of $AgAlSe_2$, the computed *B*/*G* value is 2.92, significantly exceeding 1.75. This suggests that the crystal possesses excellent ductility.

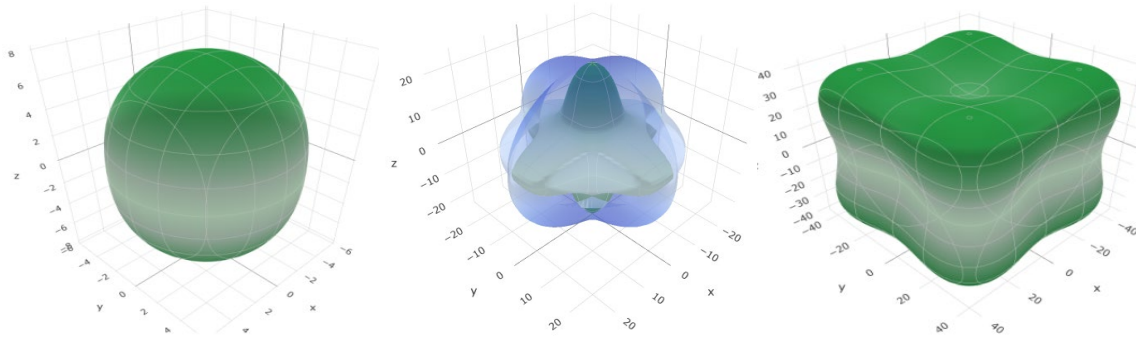

(β) *(G)* *(E)*

Fig. 3 The 3D surface contour plots of the β (TPa^{-1}), G (GPa), and E (GPa) for $AgAlSe_2$.

(β)

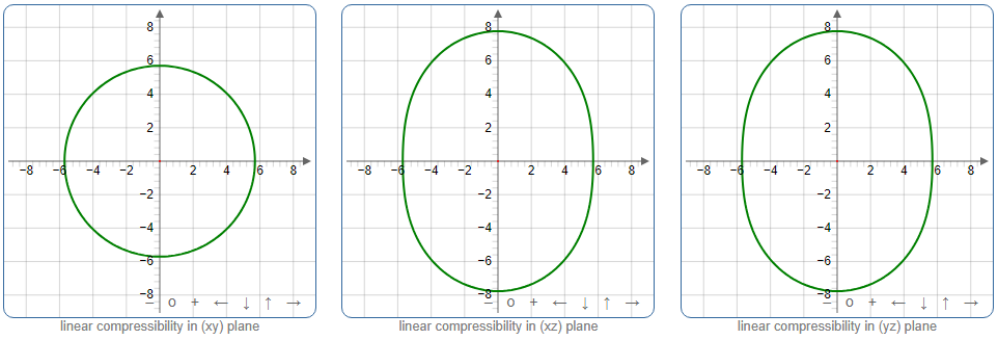

(E)

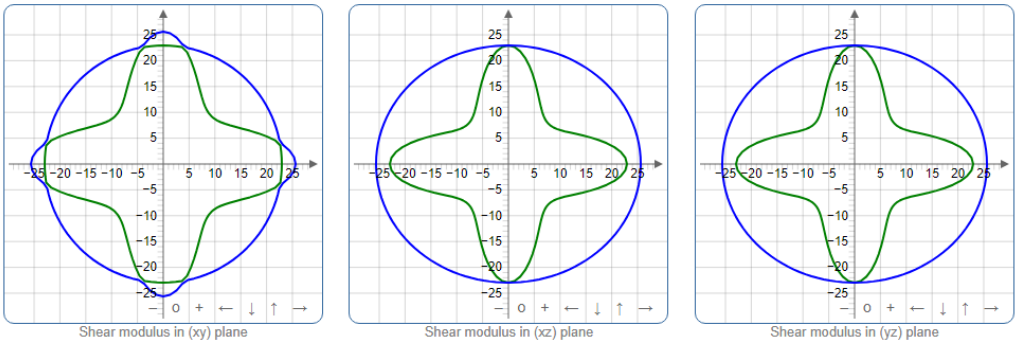

(G)

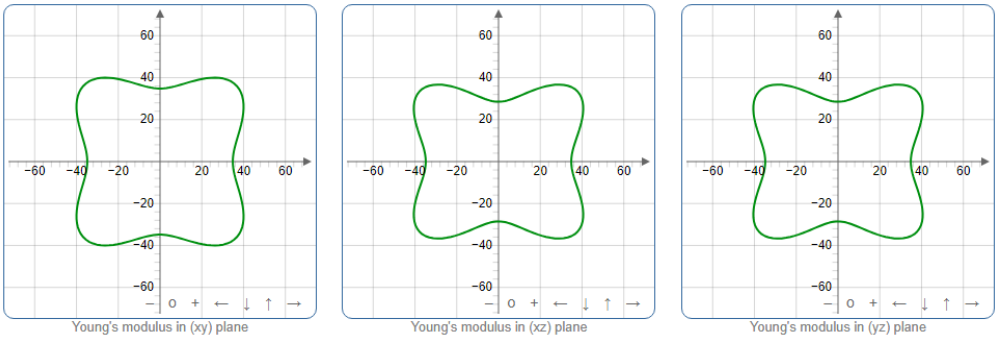

Fig. 4. The projections of the β (in TPa^{-1}), the G (GPa), and G (GPa) of $AgAlSe_2$.

Analysis of elastic anisotropy allows for the assessment of a material's mechanical properties. To quantify the elastic anisotropy index, we use the following equations [28, 29]. Here, A^U represents the overall anisotropy index, while A_B and A_G correspond to the compressibility and shear anisotropy percentages, respectively. Table 5 lists the computed values of A^U, A_B, and A_G for $AgAlSe_2$. For a perfectly isotropic crystal, these anisotropy indices would all be zero. However, the non-zero values of A^U, A_B, and A_G confirm that the material displays notable elastic anisotropy in its single crystal form.

A comprehensive understanding of elastic anisotropy in crystalline materials can be achieved by visually analyzing key mechanical properties such as linear compressibility (β), E, and G in both two-dimensional(2D) planar projections and three-dimensional(3D) spatial representations. To visualize these properties for $AgAlSe_2$, the matrix of elastic constants was fed into the ELATE software package [30-31], which generates graphical illustrations of the directional variations in E, β, and G. This visualization significantly enhances comprehension of the material's elastic characteristics. The planar and spherical graphical outputs highlight deviations from isotropy, offering clear visual evidence of anisotropic behavior. As shown in Figs. 3 and 4, the directional dependence of β, G, and E across the different planes, along with their full three-dimensional representations, is clearly depicted. To quantitatively assess the degree of elastic anisotropy, we calculated the ratios β_{max}/β_{min}, G_{max}/G_{min}, and E_{max}/E_{min}. Higher values of these ratios indicate stronger anisotropy. For $AgAlSe_2$, the computed values are: β_{max}/β_{min} = 1.362, G_{max}/G_{min} = 2.332, and E_{max}/E_{min} = 2.177. Based on both planar and 3D graphical analyses, the anisotropy strength follows the order: $\beta < E < G$, indicating that shear modulus exhibits the highest degree of directional dependence among the studied properties.

The thermal conductivity κ was computed by means of Clarke's model[32]. The Debye temperature θ, v_l, v_t, v_m is expressed through the formula [33, 34]. Moreover, the Grüneisen γ_a can be characterized in terms of the acoustic constant[35]

$$\gamma_a = \frac{3}{2}\left(\frac{3v_l^2 - 4v_t^2}{v_l^2 + 2v_t^2}\right) \tag{6}$$

The v_l, v_t, v_m, θ, κ_{min} and γ_a for $AgAlSe_2$ are summarized in Table 5, along with the results reported in Ref. [11]. By comparison, our results are in agreement with those of others, indicating the correctness of our calculations.

Table 5. Calculated v_l (km/s), v_t (km/s), v_m (km/s), θ (K), k ($W \cdot m^{-1} \cdot K^{-1}$) and γ_a of $AgAlSe_2$.

	A^U	A_B	A_G	v_l	v_t	v_m	θ	k	γ_a
This work	0.6773	0.1551	6.3163	3987	1933	2173	220.4	0.4410	2.1017
Theo.[11]				4659	2151	2401	258		

3.4. Dynamical properties

The unit cell of $AgAlSe_2$ contains 8 atoms. As a result, the phonon dispersion comprises 24 vibrational branches, which are composed of 3 acoustic modes and 21 optical modes. The optical phonon modes can be described using the following irreducible representations [36]:

$$\Gamma = 6E + 3B_2 + 3B_1 + 2A_2 + A_1 \tag{7}$$

Fig. 5 displays the phonon dispersion curve and phonon density of states for $AgAlSe_2$. The observation of exclusively no imaginary frequencies verifies the dynamic stability of the compound. The phonon dispersion reveals clear frequency gaps and can be categorized into three main groups. The high-frequency modes, located between 9 and 12 THz, are predominantly attributed to the contributions of Ag and Al atoms. In the mid-frequency region (3-6 THz), the phonon modes are also influenced by the combined of Ag and Al atoms. The low-frequency modes, within the range of 0 to 3 THz, arise from the collective contributions of Ag, Al, and Se atoms. For comparison, Table 6 presents the phonon frequencies at the Γ point for $AgAlSe_2$ alongside previously reported theoretical values from Ref. [11].

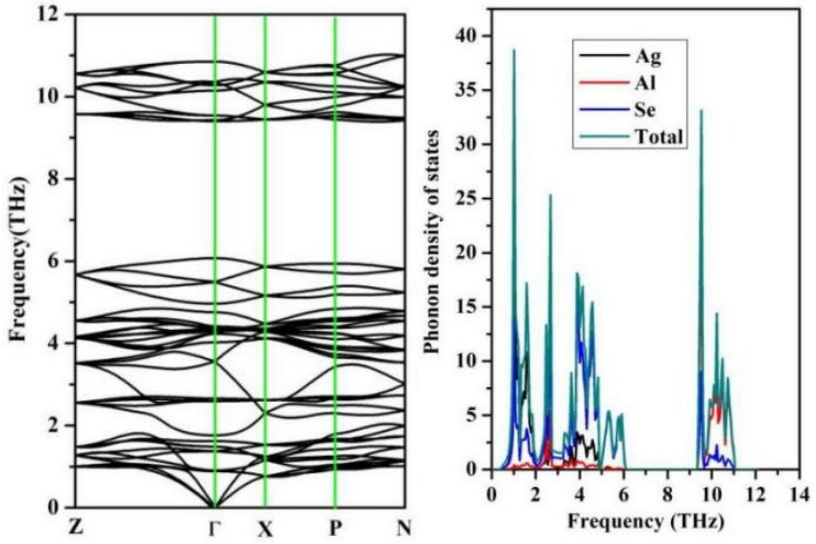

Fig. 5. Phonon dispersion curve and phonon density of states of $AgAlSe_2$.

Table 6. The phonon frequencies (THz) at the Γ point.

	6E						3B2			3B1			2A2		1A1
	E	E	E	E	E	E	B2	B2	B2	B1	B1	B1	A2	A2	A1
Present	10.28	9.54	4.38	4.23	2.66	0.91	9.43	4.41	1.76	10.15	4.75	1.62	6.07	4.32	4.96
Exp.[11]	8.90/9.62	7.43/8.78	5.45/5.60	5.15/5.27	2.97/2.88	0.84/0.78	7.82/7.82	4.86/4.86	1.83/2.07	9.02	4.95	2.19	5.63	4.35	5.54

3.5. Thermodynamic properties

Among these, Gibbs free energy (*F*), internal energy (*E*), entropy (*S*), and heat capacity (C_V) are particularly significant. These thermodynamic quantities can be precisely determined using phonon dispersion calculations combined with the density of states (DOS) approach. Under the harmonic approximation model, analytical expressions at a given temperature T are utilized to describe *F*, *E*, *S*, and C_V with high accuracy, as outlined in Ref. [37]. For the $AgAlSe_2$, Fig. 6 illustrates the phonon contributions to these thermodynamic functions. In Fig. 6(a), the C_V curve follows the expected T^3 dependence at low temperatures, consistent with theoretical predictions. As seen in Fig. 6(b), the *S* increases steadily with rising temperature across all materials considered. To further explore the thermal behavior of $AgAlSe_2$, Table 7 provides a detailed summary of its *F*, *E*, *S*, and C_V values at various temperature points.

Table 7. The calculated F (KJ/mol), E (J/mol.K), S (J/mol.K) and C_V (J/mol.K) of $AgAlSe_2$.

Temperature(K)	*F*	*E*	*S*	C_V
0	46.66	46.66	0	0
100	-2.24	92.16	471.99	345.41
200	35.06	60.98	259.21	261.45
300	-57.14	128.27	618.05	372.42
400	-124.63	166.14	726.91	383.45
500	-201.78	204.78	813.12	388.88
600	-286.75	243.83	884.31	391.92
700	-378.29	283.13	944.88	393.79
800	-475.47	322.57	997.55	395.01
900	-577.60	362.12	1044.13	395.86
1000	-684.13	401.74	1085.87	396.47

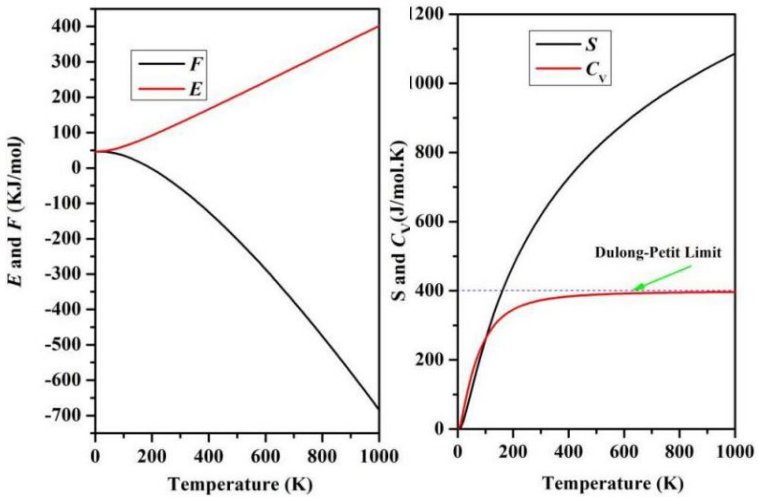

Fig. 6. Thermodynamic properties (E, F, S, C_V) for $AgAlSe_2$.

4. Conclusions

To conclude, a thorough study of $AgAlSe_2$ was conducted employing a reliable DFT method, with emphasis on its band structure, elastic characteristics, and thermodynamic properties. The material is confirmed to be a direct bandgap semiconductor. From the calculated C_{ij}, various mechanical parameters including B, G, and E were derived, providing a detailed description of the compound's mechanical response. The B/G ratio of 2.92 further supports the conclusion that $AgAlSe_2$ possesses ductile mechanical behavior. Moreover, the thermodynamic properties of $AgAlSe_2$ were also examined, offering deeper insight into its thermal stability and performance under varying temperature conditions.

Acknowledgments

This research was funded by the Technology Innovation Team of Yancheng Polytechnic College (YGKJ202503)

References

[1] D. Xue, K. Betzler, H. Hesse, Phys. Rev. B 62,13546(2000); https://doi.org/10.1103/PhysRevB.62.13546

[2] A.S. Verma, Phys. Status Solidi B 246, 192(2009); https://doi.org/10.1002/pssb.200990000

[3]R.R. Reddy, K. Rama Gopal, K. Narasimhulu, L. Siva Sankara Reddy, K. Raghavendra Kumar, G. Balakrishnaiah, M. Ravi Kumar, J. Alloys Comp. 473, 28(2009); https://doi.org/10.1016/j.jallcom.2008.06.037

[4] L.L. Kazmerski, Nuovo Cimento D 2, 2013(1983); https://doi.org/10.1007/BF02457903

[5] T. Gurel, R. Eryigit, Cryst. Res. Technol. 41, 83 (2006); https://doi.org/10.1002/crat.200410536

[6] K. Ramanathan, F.S. Hasoon, S. Smith, D.L. Young, M.A. Contreras, P.K. Johnson, A.O. Pudov, J.R. Sites, J. Phys. Chem. Solid. 64, 1495(2003); https://doi.org/10.1016/S0022-3697(03)00169-0

[7] J. L. Shay, L.M. Schiavone, E. Buehier, J.H. Wernick, J. Appl. Phys. 43, 2805(1972); https://doi.org/10.1063/1.1661599

[8] B.F. Levine, Phys. Rev. B 7, 2600(1973); https://doi.org/10.1103/PhysRevB.7.2600

[9] Hai. Xiao, Jamil. Tahir-Kheli, William.A. Goddard, Phys. Chem. Lett. 2, 212 (2011); https://doi.org/10.1021/jz101565j

[10] T. Maeda, T. Takeichi, T. Wada, phys. stat. sol. (a) 203, 2634(2006); https://doi.org/10.1002/pssa.200669539

[11] A.K. Kushwahaa, C.-G. Mab, M.G. Brikb, S. Bin Omranf, R. Khenata, Mater. Chem. Phys. 227, 324(2019)

[12] S. Mishra, B. Ganguli, Solid State Commun.151, 523(2011); https://doi.org/10.1016/j.ssc.2011.01.024

[13] Saeed Ullah, Haleem Ud Din, G. Murtaza, T. Ouahrani, R. Khenata, Naeemullah, S. Bin

Omran, J. Alloy Compd. 617, 575(2014); https://doi.org/10.1016/j.jallcom.2014.08.058

[14] A. Sharan, F. P. Sabino, A. Janotti, N. Gaillard, T. Ogitsu, J. B. Varley J. Appl. Phys. 127, 065303(2020); https://doi.org/10.1063/1.5140736

[15] G. Kresse, J. Furthmuller. Phys Rev. B 54, 11169(1996); https://doi.org/10.1103/PhysRevB.54.11169

[16] G. Kresse, D. Joubert, Phys. Rev. B 591, 758 (1999)

[17] J. P. Perdew, K. Burke, M. Ernzerhof, Phys. Rev. Lett. 77, 3865(1996); https://doi.org/10.1103/PhysRevLett.77.3865

[18] A. Togo, F. Oba, I. Tanaka, Phys. Rev. B 78 134106(2008)

[19] H. Hahn, G. Frank, W. Klingler, A. Meyer, G. Stroger, Z. Anorg. Chem. 271, 153(1953); https://doi.org/10.1002/zaac.19532710307

[20] W.N. Honeyman, K.H. Wilkinson, J. Phys. D 4, 1182(1971); https://doi.org/10.1088/0022-3727/4/8/319

[21] M. Born, K. Huang, Dynamical Theory of Crystal Lattices, Clarendon, Oxford, 1954.

[22] A.S. Verma, Sheetal Sharma, R. Bhandari, B.K. Sarkar, V.K. Jindal, Mater. Chem.Phys. 132, 416(2012); https://doi.org/10.1016/j.matchemphys.2011.11.047

[23] H. Neumann, Cryst. Res. Technol. 39, 939(2004); https://doi.org/10.1002/crat.200410280

[24] W. Voigt, Lehrbuch der Kristallphysik, Taubner, Leipzig, 1928, p. 962.

[25] A. Reuss, Z. Angew. Math. Mech. 9, 49(1929); https://doi.org/10.1002/zamm.19290090104

[26] R. Hill. Proc. Phys. Soc. Sect. A 65, 349(1952); https://doi.org/10.1088/0370-1298/65/5/307

[27] S. F. Pugh. Philos. Mag. 45, 43(1954)

[28] S. I. Ranganathan, M. Ostoja-Starzewski, Phys. Rev. Lett. 1010, 55504(2008)

[29] D. H. Chung, W.R. Buessem, F.W. Vahldiek, S.A. Mersol, Plenum, New York,1968.

[30] R. Gaillac, P. Pullumbi, F.-X. Coudert, J. Phys. Condens. Matter 28, 275201(2016); https://doi.org/10.1088/0953-8984/28/27/275201

[31] H.J. Hou, W.X. Chen, M.H. Zhu, H.Y. Wang, X.W. Lu, S.R. Zhang, Vacuum 206, 111505(2022)

[32] J. Yang, M. Shahid, C.L. Wan, J. Feng, W. Pan, J. Eur. Ceram. Soc. 37, 689 (2017); https://doi.org/10.1016/j.jeurceramsoc.2016.08.034

[33] J. Feng, B. Xiao, J. Chen, Y. Du, J. Yu, R. Zhou, Mater. Des. 32, 3231(2011); https://doi.org/10.1016/j.matdes.2011.02.043

[30] O. L. Anderson, J. Phys. Chem. Solid. 2490, 9(1963)

[34] S. Chen, Y. Sun, Y.H. Duan, B. Huang, M.J. Peng, J. Alloys Compd. 630, 202(2015); https://doi.org/10.1016/j.jallcom.2015.01.038

[35] F. Arab, F.A. Sahraoui, K. Haddadi, A. Bouhemadou, L. Louail, Phase Transit. 89, 480(2016); https://doi.org/10.1080/01411594.2015.1089574

[36] T. Hahn, International Tables for Crystallography, Space Group Symmetry, Vol. A, Reidel Dordrecht (1983).

[37] C. Lee, X. Gonze, Phys. Rev. B 51, 8610(1995); https://doi.org/10.1103/PhysRevB.51.8610